ISSN NO. 2320-5407

RESEARCH ARTICLE

Evaluation of Relatively Low Strength Maraging Steel

A. M. Reda[1] and Hossam Halfa [2]

1 Physics Department, Faculty of Science, Zagazig University, Zagazig, Egypt.
2 Steel Technology Department, Central Metallurgical Research and Development Institute (CMRDI), Helwan, Egypt.

Manuscript Info	*Abstract*
	This study aims to evaluate a new developed Maraging steel produced through air induction melting followed by electroslag remelting under CaF_2 based slag. The shielding of gamma-rays and fast neutrons by the investigated steels have been studied using Xcom and MCNP5 programs, respectively. It was found that improvement in mechanical properties of the investigated steels does not depend mainly on chemical composition but also on the production technology. This study confirmed that, high impact energy absorbed by electroslag remelting steel was being accompanied with high retained austenite percent at optimum condition of heat treatment. The microstructure results showed that, very fine and well distributed microstucture of the produced steels has been obtained after remelting using electroslag remelting process. The obtained results of shielding properties showed that, good shielding properties of steels under investigation were obtained by comparing with cobalt free titanium containing Maraging steel, 18 Ni (T200).

1. Introduction

Maraging steels have been used in a wide variety of applications including missile cases, aircraft forgings, canon recoil springs, Belleville springs, bearings, transmission shafts, coupling, hydraulic hoses, bolts and punches and dies [1- 3]. Maraging steels have been extensively used in two general applications; (a) aircraft and aerospace applications, in which the superior mechanical properties and weldability of Maraging steels are the most important characteristics, and (b) tooling applications, where the excellent mechanical properties and superior fabricatability (in particular, the lack of distortion during age hardening) are important. In the field of nuclear applications the needs for effective and cheap shielding materials are still a desirable subject. Steels are dramatically used in the reactor core, fuel transport and storage, plant structures and a lot of other nuclear uses. For the purpose of shielding, steels are very efficiently in fast neutron attenuation. For neutron attenuation calculations, the elastic and inelastic scattering reactions, and neutron capture interaction process, are of great importance [4]. The factor which determines the capability of a material to attenuate neutrons transmitted through it, is called, the macroscopic effective fast neutron removal cross-section Σ_R (cm^{-1}). The value of Σ_R can be estimated from the incident and transmitted neutron intensities, as well as the thickness of the absorber material by using Beer Lambert law [5- 10]. On the other hand, the energy deposition due to the passing of neutron through the shielding material is an important heating source. Not only the fast neutrons, but also all neutrons give rise to gamma rays heating sources, which are created when the neutrons are captured or suffering elastic scattering, this was proved by many investigators [11-14]. The advent of powerful processors and computer architectures since the early 1990's made possible the increasingly important utilization of Monte Carlo simulation programs to model complex systems, both from the point of view of the physics (type of particles and interactions, energy ranges, etc.) and from the point of view of a detailed geometrical description [15]. Wherefore, Monte Carlo simulations has rapidly increased in the space

domain, with applications ranging from instrument and detector response verification to radiation shielding optimization, component effects, support of scientific studies, and analysis of biological effects [16]. In additions, the most important quantity characterizing the penetration and diffusion of gamma-ray in a medium is the linear attenuation coefficient μ (cm^{-1}), which is defined as the probability of a gamma-rays interacting with a material per unit path length [10]. Linear attenuation coefficient divided by the mass of material gives the mass attenuation coefficient μ/ρ (cm^2/g), which is used for reference purposes. The well-known Xcom program is usually employed for calculating X-ray and gamma-ray attenuation coefficient and interaction cross sections of different material [17].

Technological properties of any material, especially shielding properties depend mainly on its chemical composition, but it was stated by many investigators that, the technological properties of steel not mainly depend on the chemical composition, but also the production technology and heat treatment conditions [18, 19].

Maraging steels are usually produced using the double vacuum melting technique [20]. Due to the high cost of the double vacuum technique, electroslag remelting technique (ESR) can be successfully used to remelt the Maraging steel and in turn improve its mechanical strength and ductility by selecting the suitable fluxes [18, 19]. The ultra-high strength of the most expensive Maraging steels is due to the precipitation of intermetallic compounds (cobalt, nickel and molybdenum) during aging process such as Ni_3Mo, Fe Mo and Fe_7Mo_6. Due to the sharp increase in the cobalt price, the development of a family of cobalt free Maraging steel is promoted. Titanium can be used as the primary strengthening element, replacing cobalt in steels [21, 22]. On the other hand, chromium was added to increase the corrosion resistance of the proposed steels. The previous are the causes of porn new Maraging steel with different mechanical and technological properties.

Since very little information is available on the properties of new developed Maraging steels specially designed for relatively low strength level applications, it was considered desirable to produce and test a series of appropriate compositions. This study aims to evaluate the new developed Maraging steel produced through air induction melting followed by electroslag remelting under CaF_2 based slag. It also aims to calculate the macroscopic effective fast neutron removal cross-section and the mass attenuation coefficient for the investigated materials with calculating the amount of energy that deposited through the shielding material due to neutron types of interactions. During the course of this work, tensile strength properties, impact energy, microstructure and shielding properties of the investigated Maraging steels were compared with the standard T200 Maraging steel.

2. Experimental work

The class of Maraging steels compromises a considerable variety of compositions, but, so far most attention has been paid to the subclass containing about 18 % nickel and particularly to those compositions capable of developing yield strengths in the range 1700 MPa to 2070 MPa when heated at optimum heat treatment conditions. Since very little information is available on the properties of Maraging steels at relatively low strength levels, it was considered desirable to produce and test a series of appropriate composition. In this study, the suggested composition was simplified variants of a composition which were recommended for use at 1380 MPa yield strength level. The nominal composition of 1380 MPa suggested material were: 12%Ni, 5%Cr, 5%Mo, and X%Ti. All other elements, particularly C, Si, Mn, S, and P, were kept at very low levels. The elemental compositions of materials of the investigated steel are shown in Table 1.

Table 1: Chemical composition of the investigated steels.

Steel No.	Condition	Chemical Composition, wt. %							
		C	Mn	Cr	Mo	Ni	Al	Ti	Fe
M9	ESR	0.0667	0.127	4.77	4.77	11.98	0.0523	0.00515	Balance
M10	ESR	0.0558	0.125	4.78	4.51	12.34	0.0716	0.163	Balance
M11	ESR	0.069	0.242	5.08	4.43	11.88	0.0001	0.32	Balance
T200	Double vacuum proces	0.02	0.05	--	3	18	0.1	0.6	Balance

2.1. Materials and methods

With the objective of this study, electroslag remelting (ESR) of new grades of low nickel, free cobalt Maraging steels under calcium fluoride (CaF_2) based slag has been investigated. Complete chemical composition analysis of the charging materials was carried out, and then melted in 100 kg induction furnace. The molten metal was casted in cylindrical ingots with diameter 75 mm and height 120 mm. These cylindrical ingots were forged and used as consumable electrodes in ESR process. Consumable electrodes were electroslag refined under pre-fused CaF_2 based flux with additions of 22.5% CaO and 25% TiO_2. Fig. 1 and 2 show the principal and solid start of the electroslag refining process [18].

Steel chips and powder of slags from different melting and refining process were collected and sampled. The Kjeldahl method was used for the determination of nitrogen on the collected samples [18].
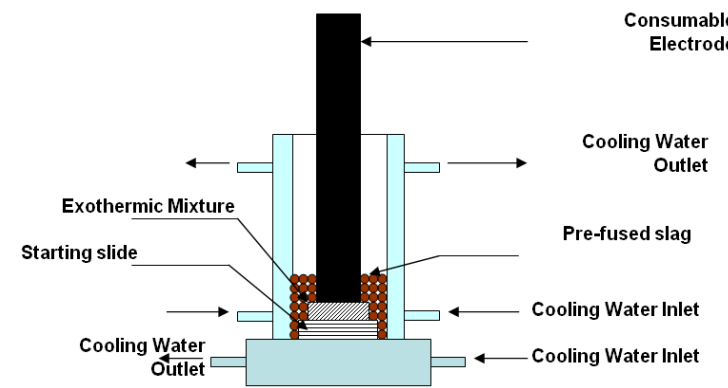
Fig. 1. Solid slag starting of ESR process.
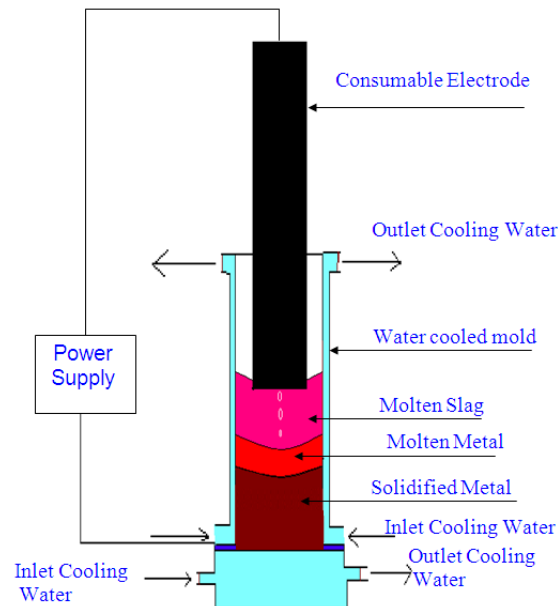
Fig. 2. Principle of ESR.

2.2. Heat Treatment Process

Strengthening of Maraging steels is achieved by soaking at a definite temperature for a definite time. Their high strength is attained by combining two strengthening mechanisms: martensitic transformation and martensitic aging. To optimize the heat treatment process (aging time and temperature) specimens from each forged steels before and after ESR were subjected to solution treatment at $820 \pm 5\ ^0C$ for one hour then air cooled (AC). The effect of variation of aging temperature (400, 425, 450, 475, 500, 525, and 550 ^0C) and time (1, 2 and 4 hrs) on hardness were established for all steels after solution annealing treatment. After optimization of aging time and temperature, which suitable for age hardening of each steel, microstructure, impact toughness and tensile specimens were aged at an optimum aging time and temperature. Microstructural characterization was performed using X-ray diffraction and metallographically by optical microscope and scanning electron microscopy.

2.3. Mechanical Properties
2.3.1. Hardness

Blocks of size 12 mm x 12 mm x 12 mm were cut from forged bar of steel under investigation produced by induction melting furnace (IF) and electroslag remelting (ESR). After carrying out the different heat treatment processes on these samples, a layer of 1 mm was removed from their surfaces to avoid the possible influence of oxygen when specimens were characterized or tested. The hardness measurements were carried out in the different heat treated steels using an **Indemtec Universal hardness-testing machine**, with 150 kg working loads, and the three readings were averaged.

2.3.2. Tension Test

The test specimen of the plane strain-tension was made according to ASTM specification E-8. The dimension of the tensile samples is shown in Fig. 3. All data reported in this investigation are averaged values of two to three tests for each of the investigated steel.

All tension testing was performed at room temperature at a crosshead speed of 0.75 mm/min. Yield strength, ultimate tensile strength, elongation and reduction of area were obtained from the axisymmetric tension test result.
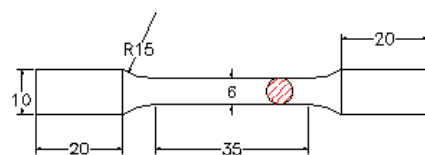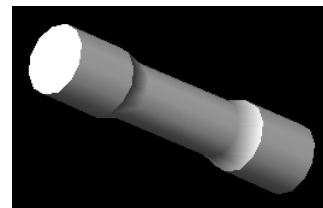
| (a)   (b) |

Fig. 3. Dimension of tension test specimen according to ASTM E-8 (a) and 3D profile of tension test specimen (b).

2.3.3. Impact Test

Standard Charpy V- notch impact specimens of 10 mm x 10 mm x 55 mm were machined along the rod, with their long axis coinciding with the length of the rod, Fig. 4. Notch of the impact specimen was cut in such a way that the crack, during the test would propagate in the radial direction.

Charpy tests were performed on an instrument impact machine of 350 J capacity and the absorbed energy was measured from the load time trace. Duplicate samples were tested corresponding for optimum heat treatment (peak-hardness) and their average value was taken. All steels under investigation were tested at 20 ^{o}C, 0 ^{o}C, -20 ^{o}C and -40 ^{o}C.

(a)   (b)
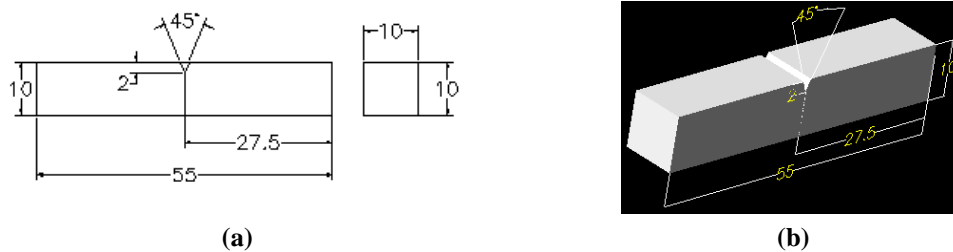
Fig. 4. Dimension of impact test specimen according to ASTM E-8 (a) and 3D profile of impact test specimen (b).

2.4. Shielding properties

Steels are a basic structure in many of nuclear construction. Therefore, the second aim of this paper is to study the shielding properties of steels under investigation. Therefore, the macroscopic effective fast neutron removal cross-section Σ_R (cm^{-1}) has been calculated using MCNP5 program [23]. Neutron isotropic point source of 14 MeV was used in the SDEF general source card for the MCNP5 input file. The continuous cross-section data library used in the program is based on the ENDF/B- VI. All experimental results for the investigated steels were compared to the traditional cobalt free titanium containing Maraging steel. In addition the total mass attenuation coefficient of the investigated materials has been calculated using Xcom program and the results were compared with the (T200) steel as in the case of neutron.

3. Result and discussions

3.1. Effect of ESR on the Mechanical Properties:-
3.1.1. Optimization of Aging Process

The chemical composition cleanliness and heat treatment of steels determine the final mechanical properties of high strength steels and particularly for Maraging steels due to Maraging operation.

The contribution of austenitizing temperature and cooling rate in strengthening the investigated steels has been clarified by previous studies [24, 25]. The data obtained in these previous investigations illustrated that neither the austenitizing temperature, 820 and 1100 °C nor the cooling rates, 0.7-3009 K/mm has a significant effect on the strengthening of the investigated cobalt free, low nickel Maraging steels. The negligible role of austenitizing temperatures 820 and 1100 °C may be explained by the high stability of both TiN and TiC. Titanium nitride is insoluble in austenite at temperature up to 1290 °C successively.

According to the results of the previous studies [24, 25], which revealed the negligible effect of higher austenitizing temperature and higher cooling rate on the strengthening of the cobalt free, low nickel Maraging steels, the investigated steels were solution treated at 820 °C for 1 h and air cooled. In steels having titanium content higher than the stoichiometric with nitrogen and carbon, a portion of titanium is left in solid solution. Due to the relatively higher solubility of titanium carbide in austenite comparing with titanium nitride, an appreciable amount of TiC is dissolved in austenite at reheating temperature (1200 °C) prior to forging process. On the other hand, a portion of titanium in solution is expected to be precipitated as a fine precipitate of TiC during and after forging causing precipitation strengthening. Furthermore, a portion of titanium in solution is precipitated during solution treatment. Consequently, in solution treatment process, TiN and TiC inhibit the austenite grain coarsening during austenitizing at 820 °C leading to finer microstructure.

In high titanium steels, titanium in solution which did not precipitate during forging and solution treatment processes is available to be precipitated during aging either as intermetallic compounds or titanium carbides and nitrides causing intermetallic and non-metallic precipitation strengthening.

To determine the aging behavior of the investigated steels, preliminary aging experiments were carried out in the range of 400 $^\circ$C to 550 $^\circ$C for 1, 2 and 4 hours after solid solution annealing for one hour at 820 $^\circ$C and followed by normal air cooling.

3.1.2. Hardness

The hardness values, ductility, strength and impact toughness of these steels are the most meaningful technological properties that determine the steel behavior. Hardness is the most often used property for testing and evaluation of steels. It is the simplest to proceed, and is a fair indication of the properties of the material.

The general influence of ESR technique and alloying element is illustrated in Fig. 5. Fig. 5 illustrates the aging curves for different Maraging steels under investigation at different aging temperatures and at different time. The hardness of the investigated steels produced in IF (induction furnace) and ESR increases as aging temperature increases, a widened peak hardness is obtained (as illustrated in Fig. 5).
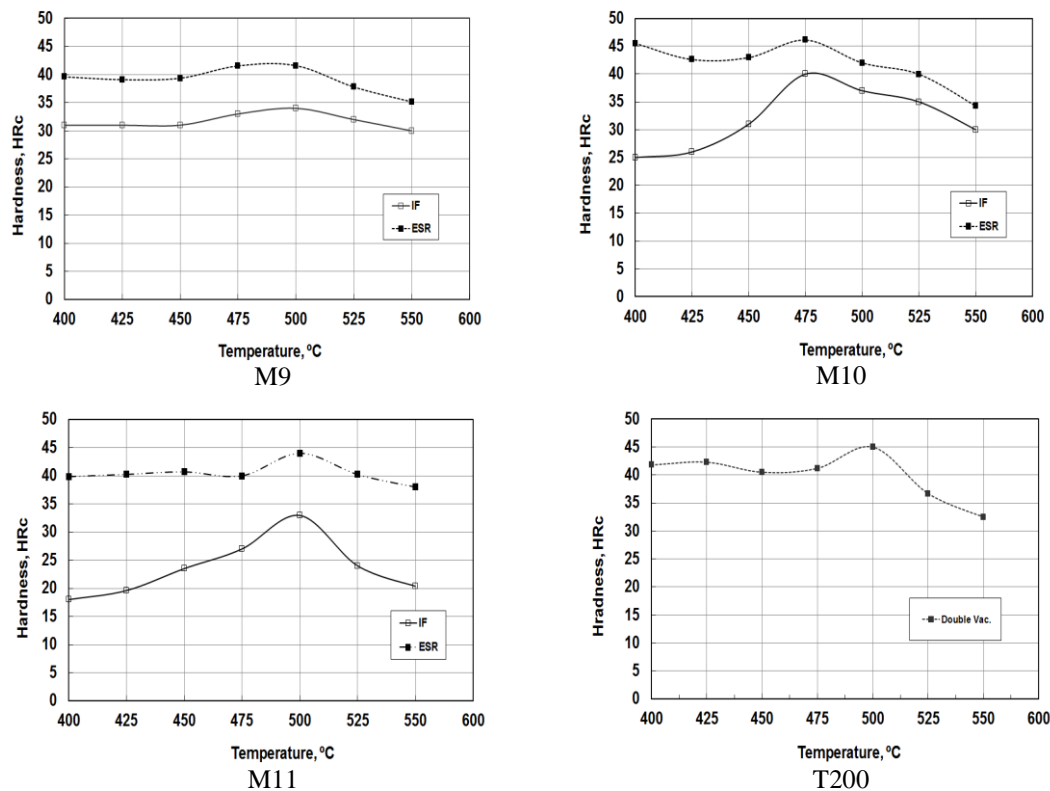
Fig. 5. Aging curves for different Maraging steels under investigation at different aging temperatures and at different time.

Further increase in aging temperature above peak aging temperature is accompanied by decreasing in hardness over-aging. From this figure, it is clear that there is a steady rise in the peak hardness level for all steels under investigation. Furthermore, it is clear from Fig. 5 that, the effect of ESR technology on aging temperature could be obtained by comparing the results obtained in the case of IF steels (air melted induction furnace) with remelted by ESR. The change of aging temperature and gain of hardness obtained by ESR technique may be attributed to increasing the percentage of intermetallic compound, decreasing the percentage of retained austenite and decreasing of grain size. The presence of these precipitates increases the strength and the hardness of the steel. From this figure, it could also be concluded that the remelting of the consumable electrodes under the CaF_2 based slag enhances the hardness profile upon aging.

3.2. Microstructure

Fig. 6 shows the microstructure of different heats of Maraging steel under investigation after optimum aging conditions. The microstructure of the investigated steel comprises martensite + retained austenite. By comparing between the microstructure of the investigated steels we found that, the structure of ESR is very finer, well distributed and free from segregation or band structure.

M9   M10   M11

a)   Induction melting, IF

M9   M10   M11

b)   Electroslagremelting, ESR

(1) As received   (2) After solution treatment   (3) After-aging

c)   Standard Maraging steel (T200)
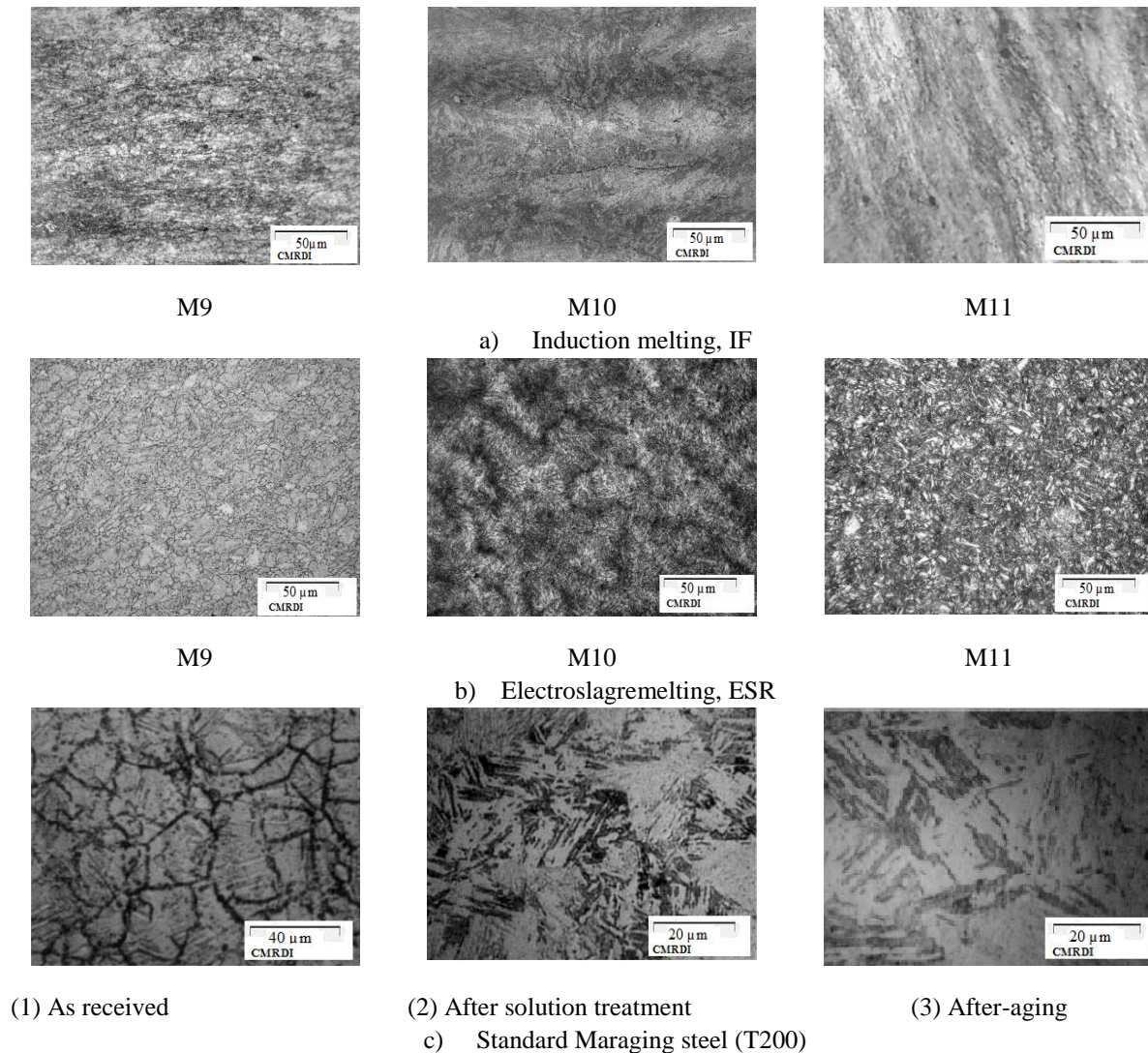
Fig. 6.Metallographical microscope observation of the investigated steels with standard (T200).

Typical optical micrographs of the material produced by IF and aged under optimum condition are shown in Fig. 6-a. The microstructure, in general appeared lamellar in morphology. The prior-austenite grain boundaries could not be resolved easily. The bright patchy regions, shown in the micrograph, correspond to regions having a considerable volume fraction of the reverted austenite. The presence of inter lath austenite, though not fully resolved, is also indicated in the microstructure.

The optical micrographs of the material produced by ESR in the peak-aged conditions are shown in Fig. 6-b. The microstructure in the peak-aged condition essentially consisted of packets of martensite, within prior-austenite grains. The austenite grains, which had transformed into packets of martensite, could still be recognized due to the

preferential etching along their boundaries and also due to the fact that the martensite packets within an austenite grain did not extend beyond the respective prior-austenite grain boundary. The martensite substructure could not be observed because of the narrowness of the martensite laths. The lathlike austenite, on the other hand, nucleates independently inside the martensite laths and also forms at the prior austenite grain boundaries. The packet-packet boundaries between the martensite laths are the preferential sites for the nucleation of recrystallization austenite. During aging of the steels under investigation the well-known precipitation reactions were occurred leading to hardening. It is generally believed that initial precipitation in cobalt free molybdenum containing Maraging steel at 480 °C occurs as Ni_3Mo, which on prolonged aging is replaced by either Fe_2Mo or the σ phase [26]. Since the alloy additionally contains titanium as a supplemental hardener, the precipitation of Ni_3Ti has also been reported; alternatively, it has been suggested that part of the titanium may be present in the molybdenum precipitate, i.e. as Ni_3 (Mo, Ti) [25- 28]. The substructure of lathe martensite consists predominantly of a high density of tangles dislocations within laths [26].

On the other hand, Fig. 6-c displays the optical micrographs of standard Maraging steel (T200) in as-received, resolution treated and subsequently aged conditions, respectively. All microstructure photographs were taken along the axis of the test specimens. Fig. 6 −c-2 and 6-c-3 show the micrographs of the T200 Maraging steel after solution treatment at 820 ºC. The slipping straps presented in the as-received state have disappeared, but the precipitates in the grain boundaries have been preserved partially. It also shows that the T200 Maraging steel is a typical lath martensite after solution treatment. That means the second phase in the as-received state did not dissolve entirely during the solution treatment. After aging, the precipitates distribute dispersively in the matrix, which contributes primarily to the second hardening effect and leads to the drastic increase in hardness.

3.3. Austenite determination

 The percentage of retained austenite influences significantly the mechanical properties of Maraging steels, limiting its usefulness as a high strength material (i.e. dual phase). Further deterioration in the mechanical properties of Maraging steels is obtained by micro-segregation of retained austenite in a localized area, i.e. the solute segregation to the existing dislocations that causes dislocation locking.

The amount of retained austenite formed after solution treatment and after aging at optimum condition for consumable electrode produced by IF and ingots produced from different heats of ESR were studied using X-ray diffraction. For IF steel, after solid solution annealing treatment at 820 °C for 1 h (air cooled), with no refrigeration treatment, about $1 \pm 0.5\%$ retained austenite was detected and X-ray diffraction results confirmed that there is a complete martensite transformation after solution-treatment of steels under investigation. On the other hand, Fig. 7, after aging, the peaks of maratensite and austenite can easily be recognized from diffraction diagram, whereas peaks of intermetallic phase such as Ni_3Ti, Fe_2Mo, Ni_3Mo are absent in this work probably because they are too dispersed and their relative volume contents are too small. Without considering precipitates, the relative contents of γ-Fe in an alloy can be easily obtained with only two phases by direct comparison method [28].

Table 2 shows measured retained austenite by X-ray diffraction method for different steels under investigation. This result clearly shows that the produced steels consist of different amounts of austenite even under the same heat treatment routines, which is obviously related to their different production technology.

It is clear from Table 2 and Fig. 7 that, the amount of retained austenite in IF melted steels depend mainly on chemical composition of the investigated steels. Increasing the amount of alloying elements, i.e. Mo, Cr, and Ti is accompanied by increasing the tendency to form retained austenite. Furthermore, the negligible effect of the ESR process on the amount of retained austenite is shown in Fig. 7. This figure clarifies that the amount of retained austenite depends mainly on its initial amount which depends mainly on its chemical compositions. On the other hand, remelting such steel using ESR process leads to uniform distribution of austenite grain (see Fig. 6). It is expected that this redistribution of the austenite grains may improve the mechanical properties.
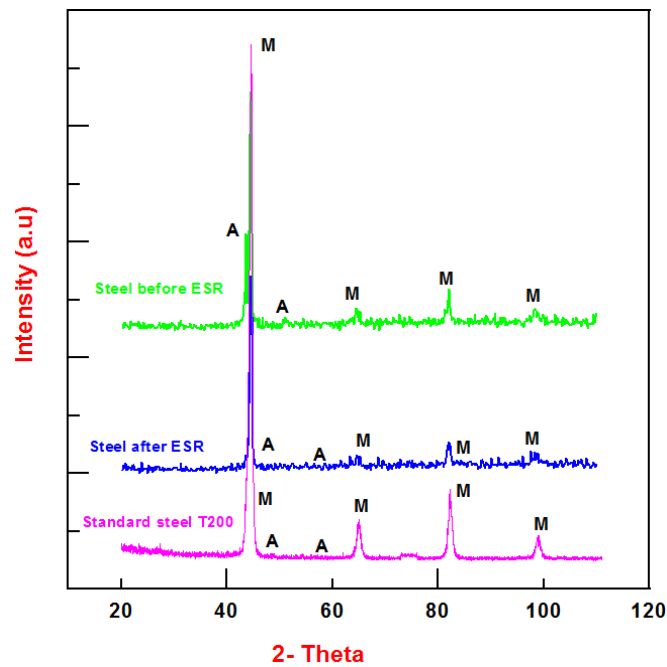
Fig. 7. X-ray diffraction pattern for the investigated steels.

Table 2: Retained austenite measured by X-ray diffraction method.

Steel No.	Process	Net austenite, %
M9	IF	7
	ESR	5
M10	IF	9
	ESR	7
M11	IF	11
	ESR	9
T200	Double vacuum process	5

It is expected that electroslag remelting of these, segregation, grain size and contamination of large NMI will be reduced. This reduction of segregation, grain size and NMI will be reflected positively on the mechanical properties (tensile ductile properties and impact toughness).

It's well known that, the behavior of steels remelted in open air induction furnace differs from that steels subjected to electroslag remelting under different flux composition. The effect of ESR flux on mechanical properties of the investigated steels is summarized in table 3. In the present study, the aging process was carried out for all the investigated steels using the optimum condition of the previous section. Table 3 represents the average result of the room temperature mechanical properties of the investigated steels after optimum aging conditions. Examination of

these results reveals the strong positive influence of ESR on the tensile ductility properties of all steels under investigation, i.e., yield, ultimate tensile strength, reduction of area and elongation.

Table 3: Mechanical properties of different steels under investigation.

Steel No.	Process	Heat treatment condition		Mechanical properties measurements				Impact energy, J		
		Temp. ºC	Time, hr	Y.S (MPa)	U.T.S (MPa)	Elong., %	Reduction of area, %	20 ºC	0 ºC	-20 ºC
M9	IF	500	4	1316	1351	15	40	21	17	18
	ESR	400	2	1465	1590	16.6	50.8	35	32	31
M10	IF	500	1	1388	1401	14	37.5	19	15	13
	ESR	475	1	1473	1530	16.2	57.1	39	32	27
M11	IF	500	1	1379	1384	12	30	34	25	25
	ESR	500	1	1427	1569	23.6	66	43	40	36
T200	Double vacuum	480	4	1449	1518	13	60	19	15	13

*All reading is average of three measurements

Maraging steel exhibited a good combination of mechanical properties like strength, ductility and impact toughness in the initial stages of overaging when i) significant coarsening of intermetallic precipitates does not occur and ii) during reversion austenite forms along the martensite lath boundaries.
The excellent toughness attained by the material could be the result of the strengthening of the matrix by the fine intermetallic precipitate and by the inherent ductility of the reverted austenite.

3.4. Impact energy
In this study, the CVN impact toughness of some cobalt free, low nickel Maraging steel has been discussed by taking into our consideration that production technology (IF or ESR) parameter, heat treatment and cleanliness of the investigated steels on impact toughness. The Charpy impact tester used does not have a built-in cooling chamber for testing at low temperature. To overcome the problem, a simple cooling container (metal container filled with special oil cooled to specified temperature using dry ice) was placed right next to the impact-testing machine. The specimen was cooled to a temperature reasonably lower than that required for CVN testing. After holding the samples at this temperature for about 10 min, to allow uniform cooling throughout, the sample was swiftly placed in the holder in the CVN machine, and the hammer was dropped. Table 3 shows the dependence of Charpy absorbed energy on temperature for steel under investigation. Also the table shows that all the investigated steels tend to have lower impact toughness as the testing temperature is decreased, but the effect is influenced by the alloy content and production technology.

Effect of ESR technology on the absorbed impact energy could be obtained by comparing the result obtained in case of air melted induction furnace with remelted by ESR. The behavior and trend of curves in Fig. 8 showed that ESR process has a positive effect on the absorbed impact energy of steel through the strong effect on decreasing the amount and area of non-metallic inclusion. It was supposed the decreasing of the amount, area and count of non-metallic inclusion leads to decrease the number of voids, which formed during application. Fig. 9 shows the fracture surface of the experimental Maraging steel in the peak-aging steel condition. The micro-morphology shows a transgranular rupture with uniform dimples due to the ductile nucleation, growth and coalescence of microvoids, (Fig. 9). The fracture surface of the standard T200 sample, as shown in Fig. 9, gives an essentially ductile behavior, though it seems to tend to be a little bit brittle, which is also accorded with high fracture toughness of the steel with ultra-high strength.
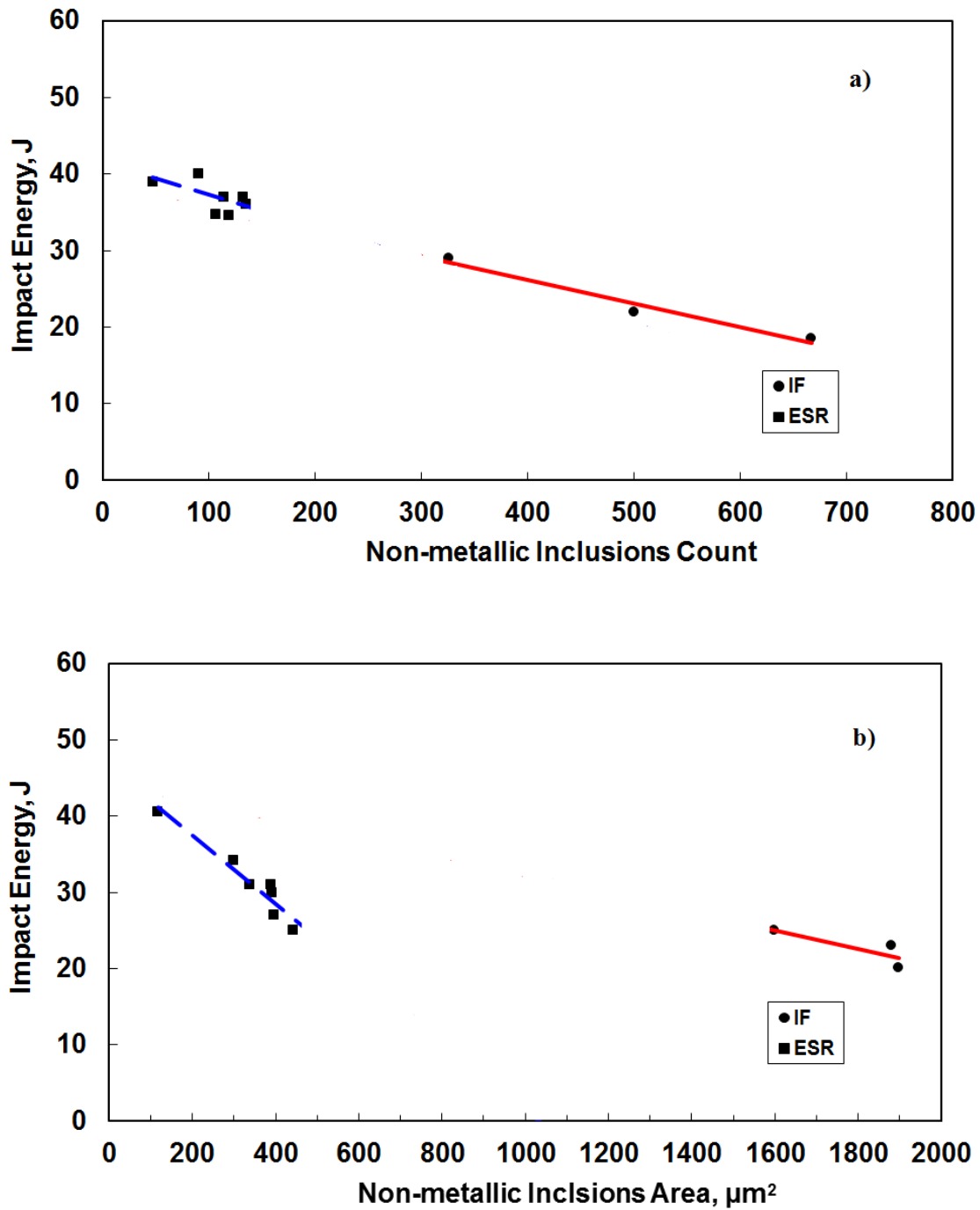
Fig. 8. The effect of non-metallic inclusions count on impact energy of the investigated steels (a). The effect of non-metallic inclusions area on impact energy of the investigated steels (b).

M9

M10

M11

T200
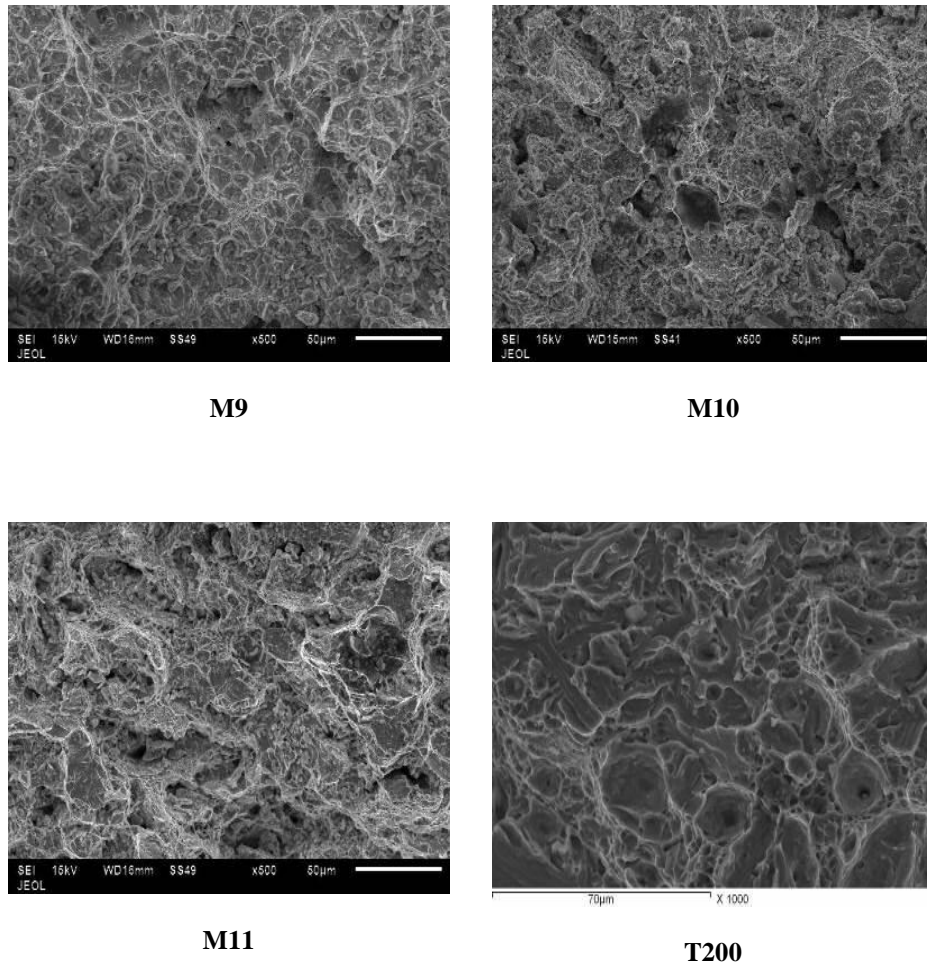
Fig. 9. Fractured surface of the investigated steels using scanning electron microscopy, SEM.

To study the effect of initial retained austenite on the absorbed impact energy at different temperatures, Fig. 10 was plotted. On the other hand, Fig. 10 illustrates the influence of initial retained austenite wt, % in impact energy absorbed by the produced steels remelted in the ESR machine as compared with initial retained austenite in consumable electrode (IF). The figure also shows that increase of retained austenite in both IF and ESR steels increase impact energy absorbed. In addition, the higher austenite contents are associated with the higher values of impact toughness. In addition, the figure shows that retained austenite is more effective in increase impact energy absorbed in case of ESR steels because the presence of very fine well distributed retained austenite between intimidate martensite lath.
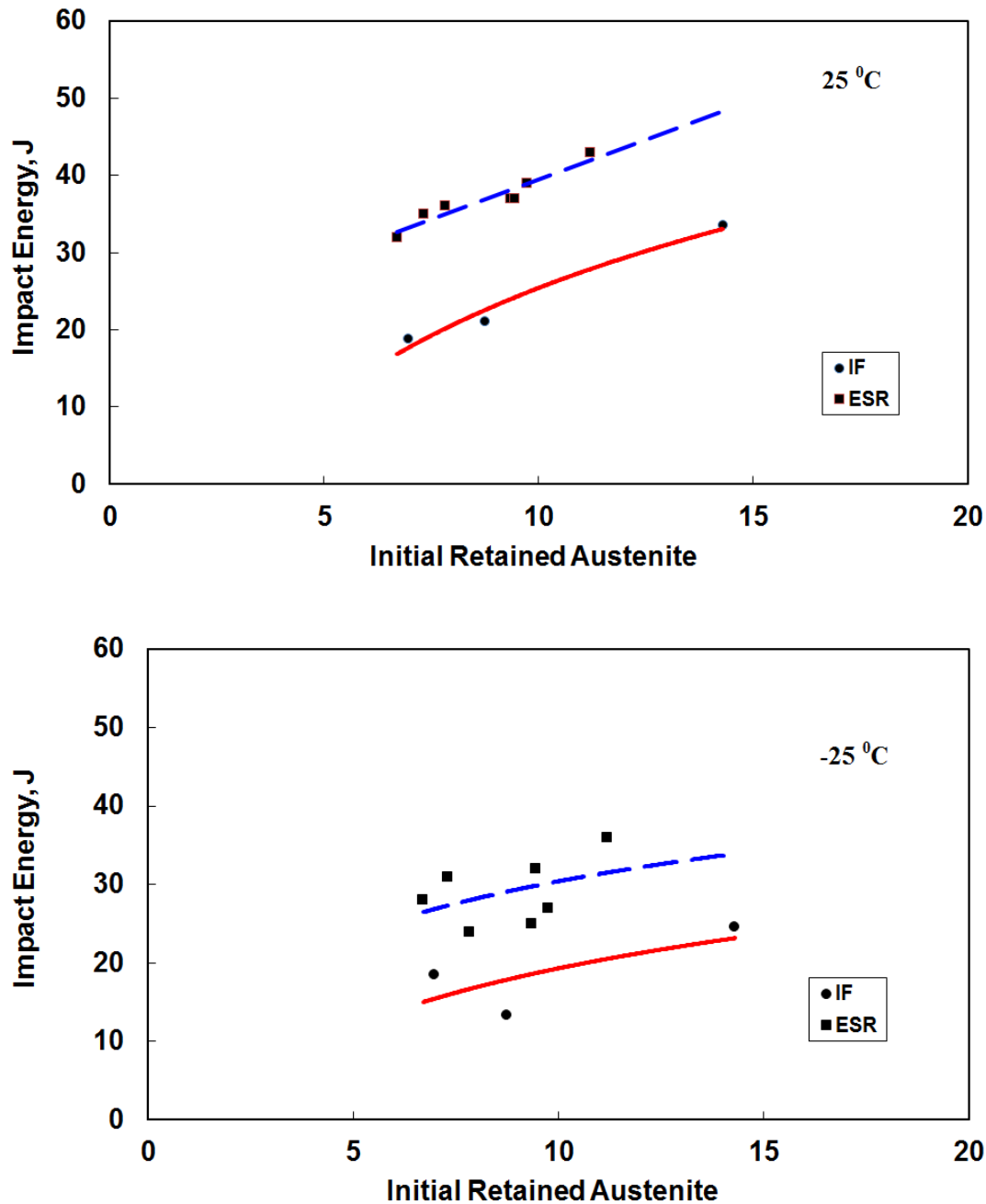
Fig. 10. The effect of initial retained austenite on impact energy of the investigated steels at different temperatures.

3.5. Shielding Properties

Calculating Σ_R for the investigated steels, aforementioned Beer Lambert law required that, mono-chromatic ray, thin absorbing material and narrow beam geometry. The experiment setup which includes the neutron source, shield of the source, neutron detector, shield of the detector and the investigated material was simulated by MCNP5 program. Tally type 4 (f4) was used to count the number of neutrons registered in the detector (neutrons/ MeV. cm^2. s). The neutron intensity with zero material thickness (I_0) and neutron intensities (I) for different thicknesses of the

investigated material were calculated. The linear relation between ln (I_0/I) versus the material thickness, that can be drawn, gives Σ_R of the investigated material. Table 4 lists the calculated removal cross-sections and the atomic densities of steel materials under investigation. As shown in table 4, the values of Σ_R are the same for all types of the tested steels. This means that, the difference in concentrations of Ni and Ti illustrated in Table 1 does not affect the ability of that steel in attenuation of neutrons. In addition, the value of Σ_R for the standard steel (T200) is approximately the same compared with the investigated steel in this study, i.e. the new developed electroslag remelted Maraging steel has the same shielding properties as the standard steel (T200).

Table 4: Effective removal cross-section Σ_R (cm^{-1}) and atom density ρ (10^{24} atoms/cm^3) for investigated steels.

Steel No.	Effective Removal Cross-section Σ_R (cm^{-1})	Atomic Density ρ (10^{24} atoms/cm^3)
M9	0.067	8.18756×10^{-2}
M10	0.067	8.20412×10^{-2}
M11	0.067	8.21191×10^{-2}
T200	0.066	8.24507×10^{-2}

On the other hand, the energy that deposited during neutron passing through the shielding material due to the different types of neutron-material interactions are shown in Fig. 11. The figure shows that, the energy transferred to the investigated material is less than the energy transferred to the standard material (T200) by approximately a factor of 1.07. This means that, the new materials can be heated less than the standard material and therefore the new material can be used in nuclear applications that required heat hold out as in the design of high power reactors.
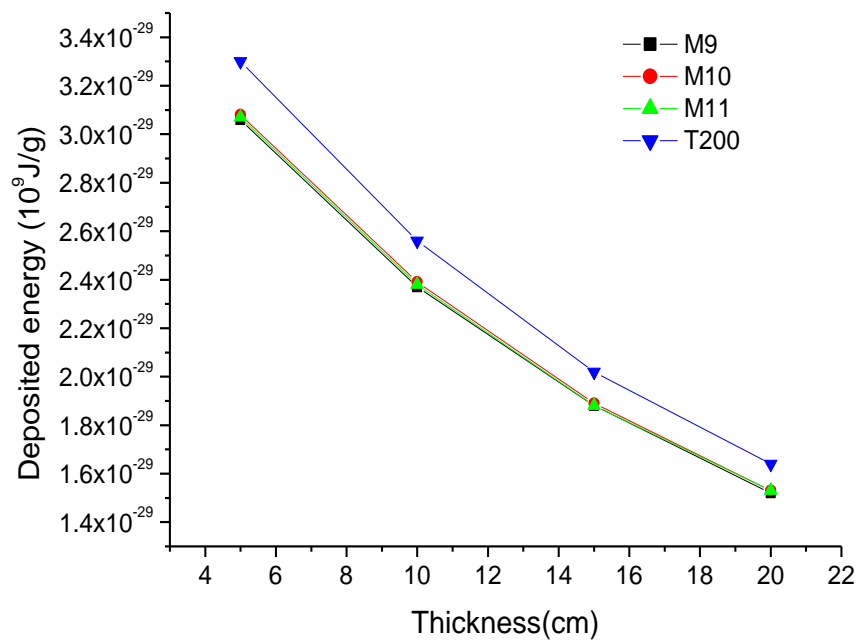
Fig. 11. The energy (10^9 J/g) deposited through different thicknesses for the different investigated steels.

The total mass attenuation coefficients of the investigated materials at photon energies of 0.01 MeV to 100 MeV have been calculated and listed in Table 5. Table 5 shows that no obvious difference in the values of μ/ρ for the investigated steels comparing among themselves and comparing with the standard T200. Also, we can note from Table 5 that the increase in the ratio of element Ti from 0.00515 to 0.6 (as shown in Table 1) for the investigated steels doesn't affect the calculated values of μ/ρ.

Table 5: Mass attenuation coefficient μ/ρ (cm^2 /g) for the new developed Maraging steel with the standard T200 at photon energies of 0.01 MeV to 100 MeV.

Photon energy (MeV)	Total mass attenuation coefficients μ/ρ (cm^2/g)			
	M9	M10	M11	T200
1.00E-02	1.70E+02	1.70E+02	1.70E+02	1.75E+02
3.00E-02	9.30E+00	9.25E+00	9.21E+00	9.15E+00
5.00E-02	2.24E+00	2.23E+00	2.22E+00	2.20E+00
1.00E-01	4.12E-01	4.10E-01	4.09E-01	4.06E-01
3.00E-01	1.12E-01	1.12E-01	1.12E-01	1.12E-01
5.00E-01	8.46E-02	8.46E-02	8.46E-02	8.48E-02
1.00E+00	6.00E-02	6.01E-02	6.00E-02	6.02E-02
2.00E+00	4.27E-02	4.27E-02	4.27E-02	4.28E-02
5.00E+00	3.17E-02	3.17E-02	3.17E-02	3.18E-02
1.00E+01	3.04E-02	3.04E-02	3.04E-02	3.05E-02
2.00E+01	3.29E-02	3.29E-02	3.29E-02	3.30E-02
3.00E+01	3.55E-02	3.55E-02	3.54E-02	3.56E-02
5.00E+01	3.93E-02	3.92E-02	3.92E-02	3.93E-02
1.00E+02	4.44E-02	4.44E-02	4.43E-02	4.45E-02

4. Conclusions

The new production technique "air induction melting followed by ESR" is a superior technique for the production of the investigated steel. This is would be due to electroslag has a great effect on decreasing the count and hence the area of non-metallic inclusions, improving the homogeneity of matrix composition, minimizing the zone segregation of alloying elements and improving the NMI distribution. In addition, the structure of ESR is very fine, well distributed and free from segregation or the band structure. Therefore, ESR process has a positive effect on mechanical properties, especially tensile strength properties and impact energy toughness of the investigated Maraging steel. All ESR steels showed higher values of the absorbed impact energy in comparison with standard steel (T200) at both room and subzero temperatures. Retained austenite is more effective in increase impact energy absorbed in case of ESR steels due to the presence of very fine well distributed retained austenite between intimidate

martensite lath. From shielding properties point of view, the investigated Maraging steel has the same shielding properties as the standard steel (T200). The energy transferred to the investigated steels are less than the energy transferred to the standard steel (T200) by approximately a factor of 1.07. Due to its attractive technological properties new developed Maraging steel can be used in nuclear construction.

References

[1] R.G. Madhusudhan et al., J. Mater. Process. Technol. 212 (2012) 66.

[2] C.R. Shamantha et al., Mater. Sci. Eng. A 287 (2000) 43.

[3] K.V. Rajkumar et al., Mater. Sci. Eng. 464 (2007) 233.

[4] M.F. Kaplan, Concrete Radiation Shielding, John Wiley & Sons, Inc., New York (1989).

[5] J.E. Martin, Physics for Radiation Protection, John Wiley& Sons, Inc., New York (2000).

[6] J.K. Shultis, R. E. Faw, Fundamentals of Nuclear Science and Engineering, 2nd.ed, CRC Press, Boca Raton, FL (2008).

[7] J.K. Shultis, R. E. Faw, Radiation Shielding, Prentice- Hall, New York (1996).

[8] Y. Elmahroug et al., Inter. J. Phys. Research (IJPR) Mar (2013) 33.

[9] Y. Elmahroug et al., Inter. J. Phys. Research (IJPR) Jun (2013) 7.

[10] A.M. El-Khayatt, Ann. Nucl. Energy 38 (2011) 128.

[11] ML Dhawan, National Conference on Radiation Shielding and Protection, Kalpakkam, India, 26–28 January (1996).

[12] M.F. Kaplan, Concrete radiation shielding, John Wiley & Sons, UK (1988).

[13] N.I. Koshim, M.G. Shirkevich, Handbook of elementary physics, Mir Publishers, Moscow (1982).

[14] M. A. Ibrahim, Ann. Nucl. Energy 29 (2002) 1131.

[15] P. Vaz, Radiat. Phys. Chem. 78 (2009) 829.

[16] G. Santin et al., Nucl. Phys. B - Proceedings Supplements 125 (2003) 69.

[17] A.M. El-Khayatt et al., Nucl. Instrum. Meth. A 735 (2014) 207.

[18] H.A. Halfa, Ph.D., Faculty of Engineering Cairo University (2007).

[19] H. Halfa et al., Steel grips, Products & Quality (2010) 278.

[20] P.W. Urzinger, et al., J. Mater. Sci. 39 (2004) 7295.

[21] V.K. Vasudevan et al., Metall. Trans. A 21 (1990) 2655.

[22] W. Sha et al., Metall. Trans. A 24 (1993) 1251.

[23] MCNP X-5, A General Monte Carlo N-Particle Transport Code, Los Alamos National Laboratory V. 5, vol. I (LA-UR-03e1987) and vol. II (LA-CP-0245) (2003).

[24] A. Fathy et al., Hradec nad Moravici, Czech. Metal (2004)1.

[25] A. Fathy et al., Steel Research 73 (2002) 549.

[26] M.L. Schmidt, In Maraging Steels: Recent Developments and Applications, the Materials, Metals & Materials Society, Edited by Richerd K. Wilson (1988) 213.

[27] J.M. Pardal et al., J. Alloys Comp. 393 (2005) 109.

[28] H. Ono et al., Metall. Mater. Trans. B (1995) 991.